Computer-Aided Civil and Infrastructure Engineering 51 (2026) 100171

Contents lists available at ScienceDirect

Computer-Aided Civil and Infrastructure Engineering

journal homepage: www.sciencedirect.com/journal/computer-aided-civil-and-infrastructure-engineering

Research Article

A physics-informed neural network (DM-PINN-FP): Incorporating cracking preference index for asphalt mixture fatigue prediction

Quan Liu [a,b,c], Huimin Li [a], Yangming Gao [b,*], Hanyu Zhang [b], Yuanyuan Li [b], Denise Lee [b], Jiantao Wu [a]

[a] College of Civil and Transportation Engineering, Hohai University, Nanjing, 210098, Jiangsu, China
[b] School of Civil Engineering and Built Environment, Liverpool John Moores University, Liverpool, L3 3AF, UK
[c] State Key Laboratory of Precision Blasting, Hohai University, Nanjing, 210024, China

ARTICLE INFO

Keywords:
Asphalt mixtures
Adhesive failure
Cohesive failure
Fatigue prediction
Viscoelastic continuum damage
Physics-informed neural network

ABSTRACT

Reliable fatigue prediction is critical to asphalt pavement design. However, most models fail to account for the dual nature of fatigue cracking, which comprises both cohesive and adhesive failure modes. To address this gap, this study presents a Dual Mode Physics-Informed Neural Network Fatigue Prediction (DM-PINN-FP) model tailored for asphalt mixtures. The adhesive failure cracking preference index (β) is quantitatively determined through pull-off tests. A Fatigue Cracking Sensitivity Index (FCSI), derived from this cracking preference index, is incorporated as a control parameter within the physics-informed network to represent the effects of aggregate type, temperature, and asphalt film thickness. Grounded in the viscoelastic continuum damage (VECD) theory, the overall damage is decoupled into adhesive and cohesive failure components, leading to coupled evolution equations for dual-mode damage. Building on these mechanisms, a dual-branch physics-informed prediction model is developed, integrating physical constraints and monotonicity conditions within a deep learning framework enhanced by multi-head attention and Long Short-Term Memory (LSTM) networks. Results show that the DM-PINN-FP model successfully mitigates cumulative error issues common in standard neural networks and substantially improves fatigue prediction accuracy. Further analysis reveals that temperature elevation predominately influences the cracking mode and accelerates stiffness degradation. Moreover, the proposed model effectively captures the impacts of different aggregate types and temperature conditions on damage progression. These findings validate the cracking preference index as a valuable link connecting mesoscopic material design parameters with macroscopic fatigue behaviors.

1. Introduction

Asphalt pavements undergo continuous accumulation of internal micro-damage under long-term repetitive loads, which progressively transitions into macroscopic cracking, ultimately resulting in the deterioration of structural performance. Fatigue cracking remains one of the most prevalent distresses in asphalt pavements. Therefore, the accurate prediction of the fatigue life of asphalt mixtures is of crucial importance for pavement structural design, material optimization, and maintenance decision-making during the service period (Hosseini et al., 2021; Underwood et al., 2010).

At present, the existing methodologies for predicting the fatigue life of asphalt mixtures are primarily categorized into phenomenological methods, fracture mechanics-based approaches, damage mechanics-based approaches, and energy-based methods(Luo et al., 2023). The phenomenological approach generally adopts S-N curves to define the load-life relationship, offering straightforward application in engineering, yet failing to elucidate the internal damage evolution. Similarly, fracture mechanics methodologies utilize the Paris law to represent cracking characteristics, but their typical exclusion of the crack initiation phase creates a discrepancy with the real-world fatigue degradation sequence (Luo et al., 2015). In contrast, damage mechanics-based approaches describe the entire process of crack initiation and propagation within a unified framework, providing a more comprehensive reflection of the damage evolution laws in the material. Within the framework of continuum damage mechanics (CDM), a fatigue model based on nonlinear damage evolution theory has been proposed (Zhang et al., 2019), while viscoelastic continuum damage theory has been applied

* Corresponding author.
E-mail address: Y.Gao@ljmu.ac.uk (Y. Gao).

https://doi.org/10.1016/j.cacaie.2026.100171
Received 25 May 2026; Received in revised form 20 July 2026; Accepted 4 August 2026
Available online 5 August 2026

to fatigue prediction of asphalt mixtures (Cheng et al., 2022). Based on the energy method, the power-law relationship between cumulative dissipated energy and fatigue life was established, which correlated the fatigue damage with cracking initiation and evolution (Shen et al., 2011). However, conventional fatigue models fail to account for the mesoscale heterogeneity of asphalt mixtures. Research indicated that fatigue cracking occurred in asphalt mixtures manifests as two distinct failure modes: adhesive and cohesive failures. Adhesive failure occurs when the local stress exceeds the interfacial strength between aggregate and bitumen. Cohesive failures describes the cracks fallen within the bitumen binder or mastics(Lytton et al., 2005). Unfortunately, existing fatigue models struggle to decouple and quantify the contribution from the above two failure modes, thereby limiting the mechanism interpretability and predictive accuracy. To address this limitation, the respective contributions of adhesive and cohesive cracking were characterized based on the surface energy decomposition of asphalt mixtures (Luo et al., 2015). The cracking criteria for adhesive and cohesive failure modes under external loading were derived, enabling the relative proportions of the two modes to be determined(Zhang et al., 2014). A multiscale approach combining coarse-grained molecular dynamics and pull-off testing was employed to investigate the effects of asphalt film thickness, loading rate, and temperature on failure modes at the bitumen–aggregate interface(Chen et al., 2022). Despite these advancements, a significant gap remains, as current findings are largely confined to theoretical discussions and lack the quantitative metrics necessary for practical fatigue life modeling.

In addition to mechanics-based approaches, data-driven methods have been extensively investigated with the advancement of computation technology and accumulation of fatigue experimental data (Chen and Liu, 2022; Shin et al., 2025; Zhu et al., 2024). Compared with conventional empirical or mechanistic models, data-driven methods can capture nonlinear relationships in high-dimensional, multi-factor-coupled datasets(Li et al., 2026). These methods have demonstrated significant potential in areas such as dynamic modulus prediction, rutting performance evaluation, fatigue life estimation, and pavement service performance analysis (Alnaqbi et al., 2024; Fahad et al., 2025; Houlík et al., 2026; Isied et al., 2019; Sun et al., 2021; Zeiada et al., 2025). Despite their advantages, purely data-driven approaches are often contingent upon the representativeness of the training datasets. They frequently encounter challenges regarding poor physical transparency and weak out-of-distribution (OOD) extrapolation, thereby limiting their robustness in engineering scenarios (Fuhg et al., 2023; Siegel, 2025; Zhu et al., 2023). In pursuit of improved generalization and physical consistency, Physics-Informed Neural Networks (PINNs) have recently emerged as a prominent research hotspot in the field of mechanical modeling (Karniadakis et al., 2021). The PINN framework incorporates governing equations, boundary conditions, and initial conditions into the network training process as loss terms, enabling the neural network to satisfy fundamental physical laws while fitting the data(Raissi et al., 2019). Fracture-mechanics prior knowledge based on the M-integral fatigue model was incorporated into the loss function as a physical constraint for predicting the fatigue life of materials containing multiple defects, achieving a correlation coefficient greater than 0.9(Dong et al., 2025). Similarly, the accuracy and extrapolation robustness of remaining useful life (RUL) prediction were significantly improved by constraining the network's output–input gradients to satisfy Paris' law, with all predictions falling within a 1.5-fold error band (Liao et al., 2025). Beyond embedding physical knowledge into loss functions and network architectures, physics-informed data augmentation strategies can be employed to address small-sample challenges. To meet the demand for accurate fatigue crack growth (FCG) prediction in the damage-tolerance design of aeroengine turbine disks, a dual-pathway PINN approach was proposed (Feng et al., 2026). By integrating experimental data with physical laws, this method overcomes the difficulty of predicting FCG under complex service conditions with limited data. In the field of pavement engineering and materials, researchers have also begun to utilize PINNs for performance evolution prediction, structural response analysis, and constitutive identification, aiming to mitigate the "high precision but weak mechanism" issue inherent in traditional data-driven models (Deng et al., 2024; Han et al., 2024; Li et al., 2025; Luo et al., 2026).

Nevertheless, current PINN-based studies largely center on the regression of macroscopic mechanics, leaving the synergistic integration of mesoscopic failure modes and macroscopic VECD equations underexplored. For this reason, this study develops a hybrid mechanics-data-driven framework for asphalt mixture fatigue prediction, embedded with a Cracking Preference Index (CPI). The methodology first defines an interfacial adhesion cracking propensity index and a fatigue cracking sensitivity index based on pull-off tests to quantitatively characterize the dominance of adhesive versus cohesive cracking under varying material and environmental conditions. Subsequently, a dual-mode damage evolution equation is established within the framework of Viscoelastic Continuum Damage (VECD) theory to describe the synergistic degradation process of interfacial and mastic damage. Finally, these physical mechanisms are embedded into a deep learning network to construct the DM-PINN-FP model, achieving high-precision prediction of the curves for asphalt mixtures.

2. Quantification of dual-mode fatigue failures

2.1. Proposal of cracking preference index

Cracking in asphalt mixtures is essentially a microscopic process of failure and debonding between the asphalt binder and aggregate (Zhang et al., 2015). Because of the stochastic nature of crack evolution, precisely calculating the true proportion of dual-mode cracking through standard experiments is challenging (Du et al., 2020). Given that the asphalt–aggregate pull-off test can distinguish adhesive from cohesive failure and reflect their relative competition under specified material and environmental conditions, this study introduces an adhesive cracking preference index, β, based on the pull-off test results. This index characterizes the relative tendency toward adhesive-dominant cracking under given compositions and environmental conditions. Accordingly, the fatigue cracking sensitivity index, R_{cr}, can be defined as:

$$R_{cr} = \frac{\beta}{1-\beta} \tag{1}$$

Where β is a dimensionless parameter related to the adhesive failure preference and ranges from 0 to 1.When $R_{cr}>1$, Adhesive cracking emerges as the predominant failure mode, with the asphalt-aggregate interface acting as the critical vulnerability for fatigue-induced damage;When $R_{cr}<1$, The failure is predominantly governed by cohesive cracking, where the inadequate resistance and fracture toughness of the asphalt binder phase constitute the main driver of crack development;In the case of $R_{cr}=1$, the contributions from both cracking modes are equivalent, indicating that the interface strength and mastic strength are in a state of relative equilibrium. Consequently, R_{cr} serves as a bridge that connects mesoscopic damage mechanisms with macroscopic fatigue responses.

2.2. Determination of cracking preference index

The cracking modes of asphalt mixtures are influenced by factors such as aggregate type, temperature, asphalt film thickness, and aggregate surface roughness (Chen, et al., 2022; Gong et al., 2025; Luo, et al., 2015; Shi et al., 2023). Therefore, in this study, pull-off tests were conducted to analyze the effects of these variables, specifically aggregate type, testing temperature, film thickness, and surface micro-texture, on the failure modes of the asphalt-aggregate interface. Digital Image Processing (DIP) technology was employed to convert the captured images of the failed interfaces into binary images. The

proportion of adhesive failure was then quantified by statistically analyzing the black and white pixel counts (Sun et al., 2020), as illustrated in Figure 1. Table 1, Table 2, Table 3 provide a summary of the pull-off test protocols and outcomes from preliminary work(Shi, et al., 2023). An unmodified bitumen with a penetration grade of 60/80 and limestone, granite, and basalt slabs measuring 100 mm × 100 mm × 10 mm were used. Three surface-texture levels were prepared using 80-mesh, 80+240-mesh, and 80+240+320-mesh polishing procedures for 10, 20, and 30 min, respectively, resulting in surface roughness values of approximately 0.0155-0.0250 mm. For each test, the bitumen mass corresponding to the target film thickness was weighed, heated to 150°C, and placed on the pull-off stub. Ten film thicknesses ranging from 10 μm to 900 μm with 100 μm intervals were taken into account as shown in Table 2. The assembled specimens were conditioned at 5, 15, and 25°C for 30 min and tested using a Pneumatic Adhesion Tensile Strength Testing Instrument (PATTI; ASTM D4541 Type IV) at a loading rate of 100 psi/s (690 kPa/s). Four replicate measurements were conducted for each combination of aggregate type, surface texture, temperature, and film thickness, yielding 1080 pull-off tests in total. It should be highlighted that the adhesive failure proportion remained at 0 for all specimens tested at 25°C.

The pull-off test results indicate that at lower temperatures, the interface failure typically exhibits mixed failure mode. As the temperature increases, the failure mode progressively transitions into a cohesive failure model. Particularly, only cohesive failure mode remains when the temperature reached 25 °C. This suggests the existence of a critical temperature T_c, above which only cohesive failure occurs (Shi, et al., 2023). The overall strength of the asphalt mixture is jointly determined by the cohesive strength of the mastic and the interfacial bond strength between the asphalt and aggregate. Although both interfacial and cohesive strengths decrease as the asphalt softens with rising temperatures (Sun, et al., 2020), the discrepancy in their decay rates triggers the observed shift in cracking mechanisms. The relationship between temperature and asphalt stiffness was described using the exponential function $y = y_0 + A_1 e^{-x/t_1}$ (Fan et al., 2024). Accordingly, the relationship between cohesive strength and temperature can be expressed as:

$$S_B = S_{B0} e^{-k_1 T} \tag{2}$$

Similarly, the relationship between interfacial bond strength and temperature can be expressed as:

$$S_I = S_{I0} e^{-k_2 T} \tag{3}$$

Then, the relationship between β and the cohesive strength and interfacial bond strength can be expressed as:

$$\beta \sim \frac{S_I}{S_B} = \frac{S_{I0}}{S_{B0}} e^{-(k_2 - k_1)T} \tag{4}$$

Specifically,

$$\beta \sim e^{-kT} \tag{5}$$

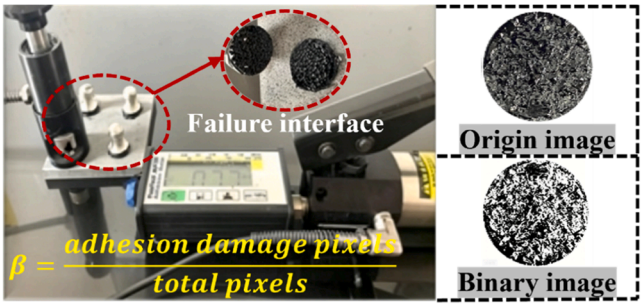

Fig. 1. Pull-off test and image processing of failed interfaces (Shi, et al., 2023).

Table 1
Test conditions for pull-off experiments.

Variables	Condition
Temperature	5°C, 15°C, 25°C
Film thickness	10 μm~900 μm
Roughness	0.0155 mm ~0.0250 mm
Aggregate type	Limestone, Basalt, Granite

Asphalt film thickness also significantly influences the failure mode. When the film is thin, pronounced stress concentration occurs at the interface, leading to failure prior to that of the mastic; as the thickness increases, cracks tend to propagate within the asphalt layer (Wang et al., 2024). This trend indicates that adhesive failure prevails when the asphalt film is sufficiently thin, whereas the failure type completely transitions to cohesive failure within the asphalt layer once the film thickness exceeds a certain threshold, h_c. That is, the β value decreases from 1 to 0 with increasing asphalt film thickness, exhibiting a monotonically decreasing S-shaped curve. To satisfy the requirements of the function's domain and range, a variant of the sigmoid function is adopted to describe this relationship:

$$\beta \sim \frac{1}{1 + a e^{b \ln h}} \tag{6}$$

Where h represents the thickness, the other parameters are constant variables.

The failure mode is also influenced by the aggregate surface roughness. The surface roughness enhances the mechanical interlocking between the asphalt and aggregate, thereby increasing the interfacial bond strength and the corresponding propensity for cohesive failure (Gong, et al., 2025; Wang, et al., 2024). As roughness increases, the change in the adhesive failure proportion varies across aggregates of different lithologies (Shi, et al., 2023). Based on the mechanisms, this study identifies temperature, film thickness, and surface roughness as the primary control variables influencing failure modes, establishing a physical model for calculating β as follows:

$$\beta(T, h, R) = cRe^{-kT} \frac{f(h) f(T)}{1 + a e^{b \ln h}} \tag{7}$$

Where T is the temperature (°C) ; h refers to the film thickness (μm) ;R represents the roughness (10^{-2} mm) ;c, k, a and b are constants;$f(h)$ and $f(T)$ are the step function (Heaviside step function) considering the critical states defined as follows:

$$f(T) = H(T) - H(T - T_c) = \begin{cases} 1, T < T_c \\ 0, T \geq T_c \end{cases} \tag{8}$$

$$f(h) = H(h) - H(h - h_c) = \begin{cases} 1, h < h_c \\ 0, h \geq h_c \end{cases} \tag{9}$$

Where T_c and h_c respectively refer to the critical temperature and thickness. When the temperature or film thickness exceeds their respective critical thresholds, the failure mode progressively transitions to being predominantly governed by cohesive failure. In the present study, T_c and h_c are treated as aggregate-specific, condition-dependent operational thresholds rather than universal constants, and their values may differ among limestone, granite, and basalt systems because of variations in mineral composition, surface characteristics, and binder–aggregate interactions. Based on the available pull-off data, T_c is constrained to $15°C < T_c \leq 25°C$, whereas h_c was not reached within the investigated film-thickness range.

2.3. Validation of cracking preference index

Based on the pull-off experimental datasets for limestone, granite, and basalt aggregates listed in Table 2 and Table 3, the model parameters were calibrated. The corresponding fitting results are presented in

Table 2
Adhesive failure proportion under varying conditions (5°C).

	Roughness/mm	Adhesive failure proportion									
		Film thickness/μm									
		10	100	200	300	400	500	600	700	800	900
Limestone	0.0165	0.41	0.40	0.39	0.35	0.29	0.25	0.18	0.16	0.11	0.12
	0.0194	0.43	0.41	0.40	0.39	0.29	0.25	0.18	0.16	0.11	0.12
	0.0237	0.62	0.56	0.51	0.46	0.33	0.31	0.29	0.18	0.19	0.20
Granite	0.0192	0.41	0.40	0.39	0.35	0.29	0.25	0.18	0.16	0.11	0.12
	0.0219	0.43	0.41	0.40	0.39	0.29	0.25	0.18	0.16	0.11	0.12
	0.0250	0.53	0.51	0.46	0.41	0.33	0.31	0.29	0.18	0.19	0.20
Basalt	0.0155	0.42	0.40	0.31	0.25	0.24	0.23	0.16	0.15	0.15	0.14
	0.0192	0.46	0.43	0.34	0.33	0.31	0.22	0.20	0.17	0.18	0.18
	0.0212	0.49	0.47	0.35	0.33	0.23	0.22	0.19	0.18	0.17	0.18

Table 3
Adhesive failure proportion under varying conditions (15°C).

	Roughness/mm	Adhesive failure proportion									
		Film thickness/μm									
		10	100	200	300	400	500	600	700	800	900
Limestone	0.0165	0.72	0.72	0.66	0.66	0.59	0.58	0.51	0.33	0.23	0.23
	0.0194	0.73	0.71	0.70	0.66	0.58	0.57	0.50	0.38	0.24	0.23
	0.0237	0.75	0.67	0.64	0.64	0.61	0.60	0.54	0.40	0.27	0.27
Granite	0.0192	0.49	0.48	0.48	0.46	0.44	0.25	0.23	0.17	0.14	0.16
	0.0219	0.55	0.51	0.46	0.41	0.33	0.31	0.29	0.18	0.19	0.20
	0.0250	0.62	0.56	0.51	0.46	0.39	0.37	0.36	0.27	0.23	0.25
Basalt	0.0155	0.45	0.43	0.36	0.33	0.26	0.24	0.19	0.20	0.17	0.18
	0.0192	0.49	0.40	0.36	0.30	0.23	0.21	0.19	0.18	0.18	0.19
	0.0212	0.52	0.50	0.45	0.37	0.25	0.21	0.18	0.17	0.17	0.19

Table 4
Fitting results for the cracking preference index.

	a	b	c	k
Limestone	4.03E-07	2.264	0.202	-0.039
Basalt	4.11E-04	1.270	0.245	-0.005
Granite	2.63E-06	2.001	0.191	-0.017

Table 4.

The results indicate that basalt exhibits the highest a value, suggesting a stronger initial sensitivity to variations in film thickness. Limestone and granite show larger b values, implying that once the film thickness reaches a certain threshold, β decreases rapidly, making the material more prone to a cohesive-dominant failure mode. The relatively small differences in c values among the three aggregate types suggest that surface roughness has a weaker influence on failure-mode preference than temperature and asphalt film thickness, consistent with previous findings(Shi, et al., 2023). Negative k values across the board suggest that the relative degradation of cohesive strength outpaces that of interfacial strength as temperature increases, favoring cohesive failure. As illustrated in Fig. 2, the proximity of most data points to the 45° line indicates a robust agreement between predictions and test results. With R^2 values exceeding 0.93 for all aggregates types and peaking at 0.98 for granite, the robustness and effectiveness of the proposed physical model are well-verified.

3. Development of the hybrid mechanics-data-driven framework

In existing fatigue life prediction methodologies, traditional mechanics-based models suffer from limitations in mechanistic insight and predictive accuracy, while purely data-driven models lack physical interpretability and generalization capabilities. To address these issues, this study proposes a mechanics-data dual-driven fatigue life prediction model for asphalt mixtures that embeds the Cracking Preference Index, termed DM-PINN-FP (Dual-mode Physics-Informed Neural Networks for Fatigue Prediction). This model embeds the evolution equations of dual-mode VECD theory and monotonicity constraints into the network training process, leveraging deep learning to extract complex temporal non-linear features and achieve the separation and precise prediction of macroscopic C-S curves. This whole procedure encompasses three sections: 1) VECD method considering different cracking modes; 2) the dual-driven fatigue prediction framework; and 3) the construction of the physics-informed loss function.

3.1. Dual-mode viscoelastic continuum damage (VECD) theory

Although the conventional VECD model successfully reflects the global fatigue evolution through a single damage variable, while it lacks the resolution to differentiate between failure mechanisms. In this study, a cracking preference index correlated with material strength, is incorporated into the VECD framework. Acting as a governing parameter for damage evolution, it allows for the quantitative representation of the competitive interplay and relative dominance between interfacial and cohesive cracking modes. To incorporate the dual-mode competition, the total damage in this work is decoupled into cohesive and adhesive components. Specifically, cohesive damage is characterized using Linear Amplitude Sweep (LAS) testing (Błażejowski et al., 2020), where the pseudo-strain of the asphalt binder is expressed as:

$$\varepsilon^R = |G^*|_{LVE}\varepsilon_0 \tag{10}$$

Where $|G^*|_{LVE}$ is the linear viscoelastic complex modulus, ε_0 refers to the initial strain.

The pseudo-stiffness of the asphalt binder, C_{co}, is defined as the normalized complex shear modulus (Cao et al., 2019):

$$C_{co} = \frac{|G^*|_i}{|G^*|_{LVE}} \tag{11}$$

Where $|G^*|_i$ refers to the complex modulus at the i-th loading cycle. i

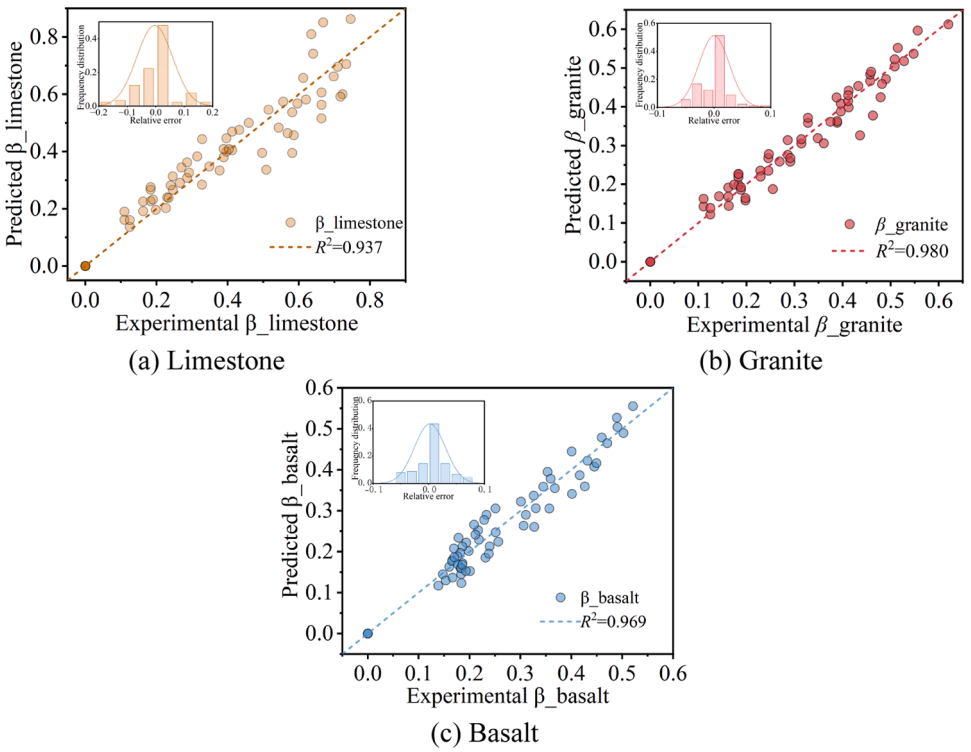

Fig. 2. Model prediction performance and error distribution for CPI.

means the number of cycles.

According to the Schapery theory (Park et al., 1996), the relationship between damage evolution rate and energy dissipated rate in the fatigue process can be expressed as follows:

$$\frac{dS_{co}}{dt} = \left(-\frac{\partial W_{co}^{R}}{\partial S_{co}} \right)^{\alpha_1} \tag{12}$$

Where S_{co} is the damage parameter corresponding to cohesive damage; W_{co}^{R} is the pseudo-strain dissipated energy corresponding to cohesive damage; and α_1 is the damage evolution rate determined by the relaxation curve of the asphalt binder.

The damage parameter S_{co} is calculated as follows:

$$S_{co}(t) = \sum_{i=1}^{N} \left[\frac{1}{2} \left(\varepsilon^{R} \right)^2 \left(\mathrm{C}_{co}^{i-1} - \mathrm{C}_{co}^{i} \right) \right]^{\alpha_1/1+\alpha_1} \left(t_i - t_{i-1} \right)^{1/1+\alpha_1} \tag{13}$$

For interfacial adhesive damage, isolating the interfacial damage from the material damage and establishing a damage variable that reflects the actual interfacial stress state remain significant challenges in current research. Within the framework of viscoelastic continuum damage mechanics, and following the formulation of cohesive damage, the interfacial pseudo-strain can be defined as:

$$\gamma^{R} = |K^{*}|_{LVE} \gamma_0 \tag{14}$$

Where $|K^{*}|_{LVE}$ is the initial linear viscoelastic (LVE) complex shear stiffness when the interface is undamaged. γ_0 is the initial shear strain.

The interfacial pseudo-stiffness, C_{ad}, is used to characterize the degradation of the adhesive integrity at the asphalt-aggregate interface with respect to the number of loading cycles, and is defined as:

$$C_{ad} = \frac{|K^{*}|_i}{|K^{*}|_{LVE}} \tag{15}$$

Where $|K^{*}|_i$ is the interfacial dynamic shear stiffness at the i-th loading cycle.

The evolution of the interfacial damage variable, S_{ad}, likewise follows Schapery's damage evolution law:

$$\frac{dS_{ad}}{dt} = \left(-\frac{\partial W_{ad}^{R}}{\partial S_{ad}} \right)^{\alpha_2} \tag{16}$$

Where W_{ad}^{R} is the pseudo-strain dissipated energy corresponding to the interfacial adhesive damage. α_2 is the interfacial damage growth rate parameter.

The derivation of the calculation formula for the internal interfacial damage variable, S, during cyclic loading is as follows:

$$S_{ad}(t) = \sum_{i=1}^{N} \left[\frac{1}{2} \left(\gamma^{R} \right)^2 \left(\mathrm{C}_{ad}^{i-1} - \mathrm{C}_{ad}^{i} \right) \right]^{\alpha_2/1+\alpha_2} \left(t_i - t_{i-1} \right)^{1/1+\alpha_2} \tag{17}$$

In summary, this study treats the total damage as a linear coupling of interfacial adhesive damage and mastic cohesive damage, and proposes the following dual-mode damage evolution equation:

$$\frac{dS}{dt} = \beta \left(-\frac{\partial W_{ad}^{R}}{\partial S_{ad}} \right)^{\alpha_2} + (1-\beta) \left(-\frac{\partial W_{co}^{R}}{\partial S_{co}} \right)^{\alpha_1} \tag{18}$$

In which S denotes the internal damage variable of the asphalt mixture. β represents the weighting coefficient governing the coupling between adhesive and cohesive damage modes. It characterizes the relative dominance of the two failure mechanisms under a given material state and is determined using the pull-off-test-based physical model described in Section 2.2; therefore, it should not be interpreted as the actual proportion of adhesive cracking.

3.2. A hybrid mechanics-and-data-driven fatigue architecture

Based on dual-mode damage theory, the DM-PINN-FP framework decouples total damage into interfacial adhesive and mastic cohesive components. It regulates the relative roles of these two modes through the fatigue cracking sensitivity index (R_{cr}) and embeds monotonicity conditions into the network training process to achieve precise prediction of the C-S curves for asphalt mixtures. As illustrated in Fig. 3, the architecture of DM-PINN-FP comprises an input layer, a deep feature

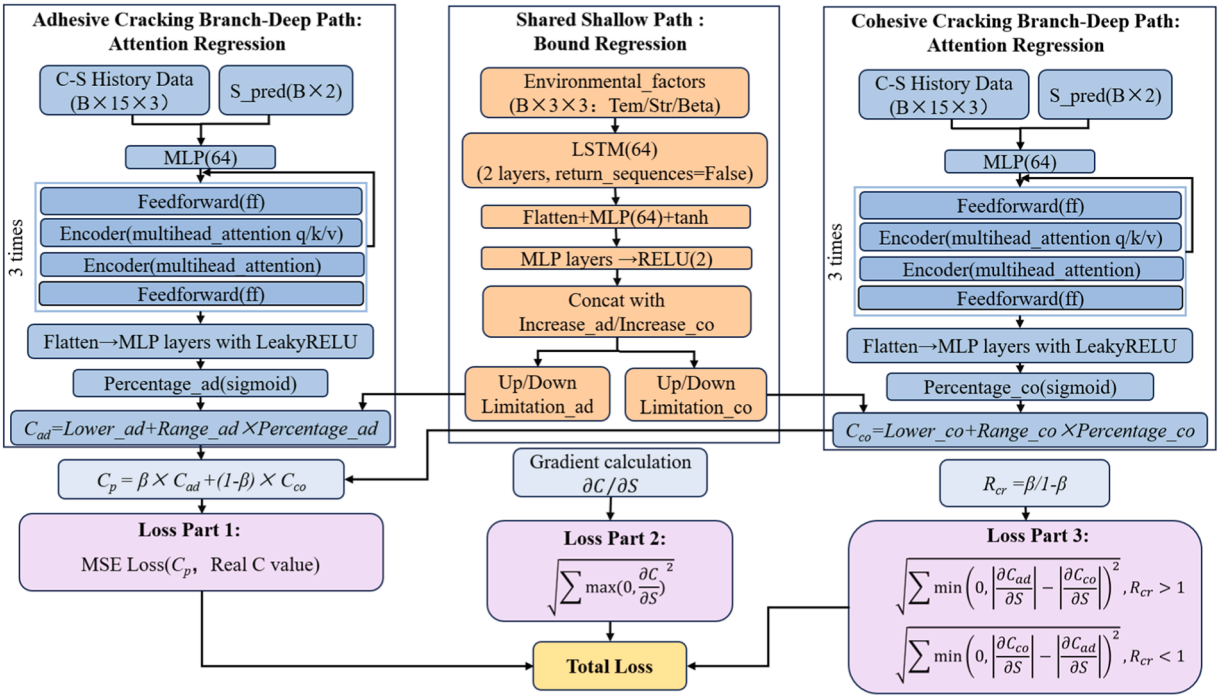

Fig. 3. Architecture of DM-PINN-FP.

mapping layer, dual-mode physical branch layers, and a physical boundary constraint layer. At the input terminal, the data consists of three components:

(1). Historical sequences from the preceding L time steps (C, S, β), used to characterize the damage accumulation path of asphalt mixtures.
(2). Damage state of the target point (S_p, β), used to locate the current prediction point within the damage evolution process.
(3). Environmental state tensors, including external variables such as strain levels, temperature, and the cracking preference index (β), reflecting the operational dependency of the asphalt mixture's fatigue behaviour.

During the feature extraction phase, the model employs a deep fully connected network integrated with a multi-head attention mechanism to encode the input sequences, capturing key features and long-range dependencies in damage evolution across different loading stages. This module consists of five fully connected layers, each containing 64 neurons with ReLU activation, followed by a multi-head attention layer with eight attention heads and a key dimension of 16. The multi-head attention mechanism enhances the model's ability to identify local mutations and phase-wise degradation characteristics, thereby improving its representation of complex non-linear C-S curve morphologies. The resulting shared feature representation is then passed to two symmetrical but parameter-independent physical branches: an interfacial adhesive branch for predicting C_{ad} and a mastic cohesive branch for predicting C_{co}. This dual-branch structure reduces the aliasing of adhesive and cohesive damage mechanisms within a single latent representation. The outputs of the two branches are subsequently weighted and combined according to the dual-mode coupling equation to obtain the predicted pseudo-stiffness C_p at the target time step. To further ensure the physical validity and temporal stability of the predictions, a shared physical-boundary pathway is incorporated. This pathway consists of two stacked Long Short-Term Memory layers with 64 hidden units per layer and recursively integrates the historical states. Its hidden states preserve the accumulated damage history and dynamically estimate the physically admissible upper and lower bounds of pseudo-stiffness at the target step. Compared with a prediction framework based solely on deep feature fitting, this pathway suppresses nonphysical deviations caused by error accumulation during recursive prediction and thereby improves the long-term stability and robustness of the model.

3.3. Formulation of the physics-informed loss function

To ensure the model strictly adheres to the principles of continuum damage mechanics, the total loss function of the DM-PINN-FP is formulated by integrating traditional data-driven loss with physics-based constraints. The loss function is generally defined as a metric of the prediction error between the model output and the ground truth, with a lower loss value indicating superior predictive performance. The core advantage of DM-PINN-FP lies in its integrated approach; it accounts not only for the deviation between predicted and experimental values but also incorporates physical knowledge derived from VECD theory and the cracking sensitivity index. This ensures that the network not only fits the experimental C-S data but also maintains physical interpretability even in regions with sparse data. The mathematical descriptions of this prior physical knowledge are summarized in Table 5.

Because pseudo-stiffness decreases with increasing damage, the admissible sign convention is $\partial C/\partial S < 0$. The monotonicity loss therefore penalizes positive values of $\partial C/\partial S$. The branch-specific degradation rates are defined by their non-negative magnitudes. The total loss function consists of two components: a data-driven loss ($Loss_D$) derived from observational data, and a physics-based loss ($Loss_P$) rooted in prior physical knowledge. The $Loss_D$ is calculated using the Mean Squared

Table 5
Mathematical formulations of prior physical constraints for fatigue failure.

Expressions	Prior physical knowledge
$\frac{\partial C}{\partial S} < 0$	C decreases as S increases
$\left\|\frac{\partial C_{ad}}{\partial S}\right\| > \left\|\frac{\partial C_{co}}{\partial S}\right\|$	When $R_{cr} > 1$, the stiffness degradation rate of the adhesive branch is higher
$\left\|\frac{\partial C_{co}}{\partial S}\right\| > \left\|\frac{\partial C_{ad}}{\partial S}\right\|$	When $R_{cr} < 1$, the stiffness degradation rate of the cohesive branch is higher

Error (MSE) loss function, while the derivatives within the physics loss term are computed using the automatic differentiation technique within the TensorFlow framework. The output value of the combined loss function depends on the degree to which established physics knowledge is violated. When the value of the physics loss term reaches zero, the fatigue predictions provided by the network perfectly adhere to the physical principles prescribed in Table 5. The total loss function is formulated as follows:

$$Loss_D = MSELoss(C_p, C) \tag{19}$$

$$Loss_{mono} = \sqrt{\sum \max\left(0, \frac{\partial C}{\partial S}\right)^2} \tag{20}$$

$$Loss_{mode} = \begin{cases} \sqrt{\sum \min\left(0, \left|\frac{\partial C_{ad}}{\partial S}\right| - \left|\frac{\partial C_{co}}{\partial S}\right|\right)^2}, R_{cr} > 1 \\ \sqrt{\sum \min\left(0, \left|\frac{\partial C_{co}}{\partial S}\right| - \left|\frac{\partial C_{ad}}{\partial S}\right|\right)^2}, R_{cr} < 1 \end{cases} \tag{21}$$

$$Loss_P = Loss_{mono} + Loss_{mode} \tag{22}$$

$$Loss = \lambda_1 Loss_D + \lambda_2 Loss_P \tag{23}$$

Where $Loss_{mono}$ denotes the monotonicity penalty and $Loss_{mode}$ denotes the mode cracking-consistency penalty, together, they constitute the physics-based loss term. λ_1 and λ_2 are hyperparameters to maintain a balance between data and physical constraints.

4. Results and discussion

4.1. Model training and convergence analysis

The model was trained and tested using four-point bending fatigue data for an AC-25 asphalt mixture containing limestone aggregate(Han, et al., 2024). The experimental conditions and calculated β values for the 18 obtained C-S curves are summarized in Table 6. For a given asphalt mixture, the average asphalt film thickness and aggregate surface roughness remain constant, with the calculated values of h=9.1 μm and R= 0.02 mm, respectively. Therefore, β was treated as a temperature-dependent parameter in the present study, and the same β value was assigned to different strain levels and loading frequencies at a given temperature. The β values in Table 6 are introduced as a strength-related cracking-preference prior rather than as the adhesive crack-area fraction of the fatigue specimen. The adhesive–cohesive failure pattern observed in pull-off tests reflects the relative competition between interfacial adhesion and binder or mastic cohesion, both of which are closely related to mixture fatigue performance(Azarhoosh et al., 2017; Cong et al., 2017; Kim et al., 2004; Lucas Júnior et al., 2020). In the dual-mode VECD framework, β regulates the relative contributions of the two damage branches, while their degradation behavior is learned from the mixture-scale C-S curves. Thus, β provides a mechanism-informed cross-scale coupling parameter rather than a direct geometric mapping of crack areas.

In this study, two complete C-S curves corresponding to 25°C-400 με-5 Hz and 25°C-400 με-10 Hz were withheld prior to sliding-window sample generation and used exclusively for final testing. The remaining 16 curves were used to construct the training and validation datasets. Specifically, each curve was segmented using a 16-point time series window, with the first 15 points serving as model inputs and the 16th point as the corresponding prediction target. The resulting samples were then randomly divided into training and validation subsets at a ratio of 4:1. Although the individual temperature, strain, and frequency levels represented in the test cases were present elsewhere in the training data, the coupled condition of 25°C and 400 με was excluded. Therefore, this data split was designed to evaluate the model's generalization capability for an unseen temperature–strain combination located at the boundary of the investigated domain. All neural networks in this study were implemented based on the TensorFlow deep learning framework. During the training stage, a sequential optimization strategy combining the Adam optimizer and the L-BFGS second-order optimizer was adopted (Mazeika et al., 2024). Adam was utilized in the initial stage to rapidly escape local minima, while L-BFGS was employed in the later stage to achieve high-precision fitting. The core training hyperparameters are summarized in Table 7. The loss function was recorded every 10 epochs, and the epoch with the minimum training loss was saved as the optimal model for subsequent prediction of complete C-S curves.

Table 6
Experimental conditions [29] and calculated values of β.

Temperature/°C	Loading frequency/Hz	Strain level/με	β/-
5	5, 10	200, 300, 400	0.48
15	5, 10	200, 300, 400	0.7
25	5, 10	200, 300, 400	0

Fig. 4 illustrates the convergence trends of the loss terms during training and validation. When the proportions of $Loss_D$ and $Loss_P$ in the total loss differed (i.e., λ_1= 1 and λ_2= 0.1), Fig. 4 (a) and (b) show that $Loss_D$ rapidly converged to near zero within the first 50 epochs, whereas $Loss_P$ failed to exhibit significant convergence even after 50 epochs. This discrepancy suggests that optimizing $Loss_P$ is more challenging than $Loss_D$. Increasing the proportion of $Loss_P$ (settingλ_1= 1 and λ_2= 1) effectively addressed this issue. As shown in Fig. 4 (b), $Loss_P$ gradually decreased and eventually converged around the 30th epoch. Furthermore, Fig. 4 (d) confirms that the validation loss also converged to near zero after 50 epochs, validating the effectiveness of the selected weighting parameters.

4.2. Model validation and predictive capability

To validate the DM-PINN-FP model proposed in Section 3, its predictive performance was compared with that of a conventional Artificial Neural Network (ANN) (Ulloa et al., 2023). To ensure a fair comparison, both models used identical input sequences, data preprocessing procedures, training and test splits, batch sizes, and optimizer settings. The ANN architecture, illustrated in Fig. 5, consists of an input layer, five fully connected hidden layers, and an output layer. Each hidden layer

Table 7
Hyperparameters and implementation details for DM-PINN-FP.

Type	Hyperparameter	Value
Training	Train ratio	0.8
	Total epoch	100
	Optimizer	Adam, L-BFGS
	Adam batch size	4
	Adam Learning rate	0.0001
	Adam training epochs	20
	L-BFGS batch size	Full batch
	L-BFGS step-size setting	Adaptive Hager–Zhang line search; initial step size = 1.0
	Loss function	MSE loss
	λ_1, λ_2	1, 1
Network structure	Hidden layers in each adhesive/cohesive branch	3 Multi-Head Attention layers, 2 Feedforward layers, and 5 Fully connected hidden layers
	Attention modules per branch	3
	Number of attention heads	8
	Attention dropout rate	0.1
	Sizes of Feedforward layers	128
	Sizes of Fully connected layers	64
	LSTM units per layer	64

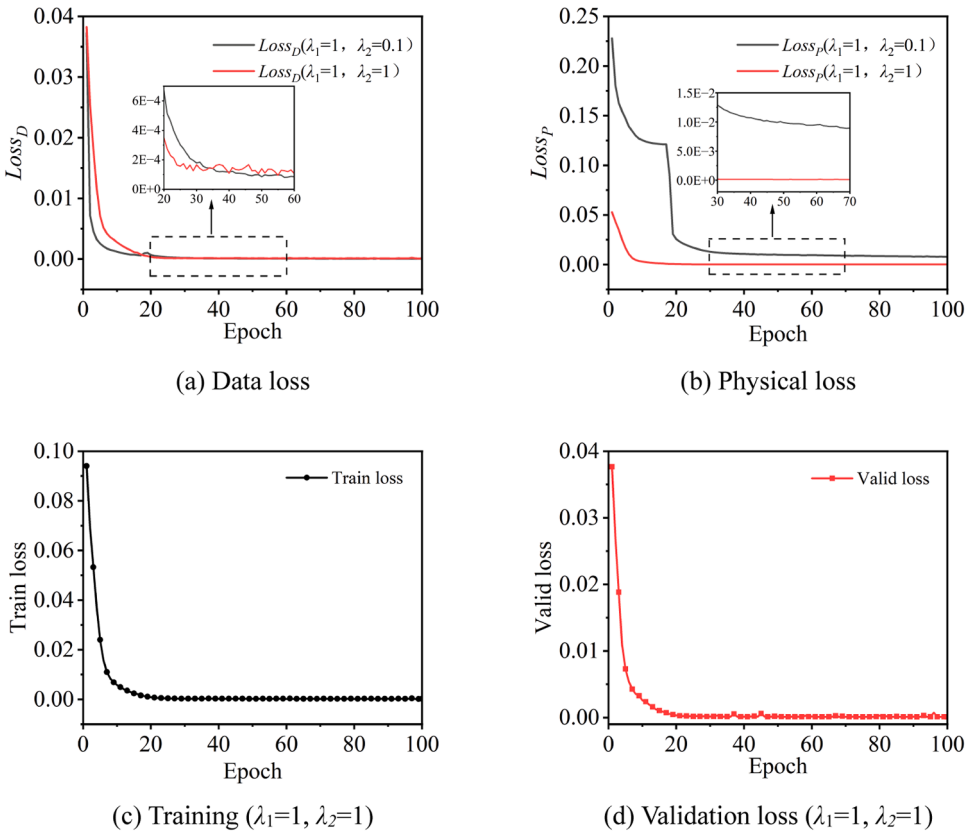

Fig. 4. Loss monitor in the model training and validation.

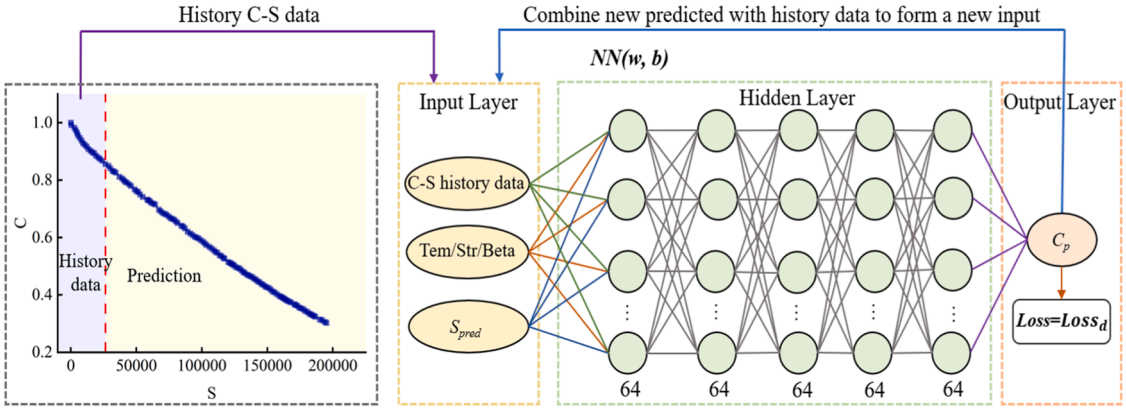

Fig. 5. Framework of ANN model.

contains 64 neurons, matching the depth and width of the shared fully connected feature-mapping module in DM-PINN-FP. The input layer is consistent with that of DM-PINN-FP, while the output layer provides the predicted pseudo-stiffness C_p at the target point C. In contrast to the ANN, the additional multi-head attention module, dual physical branches, and recurrent physical-boundary pathway in DM-PINN-FP are specifically introduced to represent the proposed dual-mode damage mechanism and impose the associated physical constraints. The ANN loss function is expressed as:

$$Loss_d = MSELoss(C_p, C) \tag{24}$$

Table 8 lists the evaluation metrics for both models on the validation set. Fig. 6 displays the prediction accuracy of the two models for the 5 Hz and 10 Hz validation samples. As indicated in Table 8, the proposed DM-PINN-FP model achieves the minimum values in both RMSE and MAE, whereas the purely data-driven ANN model exhibits relatively larger errors. In Fig. 6, the horizontal axis represents the experimental C

Table 8
Evaluation metrics of DM-PINN-FP and ANN on the validation set.

	DM-PINN-FP	ANN
Case a: 5Hz - validation set		
RMSE	0.0075	0.0353
MAE	0.0058	0.0263
R-square	0.9990	0.9547
Case b: 10Hz - validation set		
RMSE	0.0080	0.0295
MAE	0.0063	0.0262
R-square	0.9989	0.9624

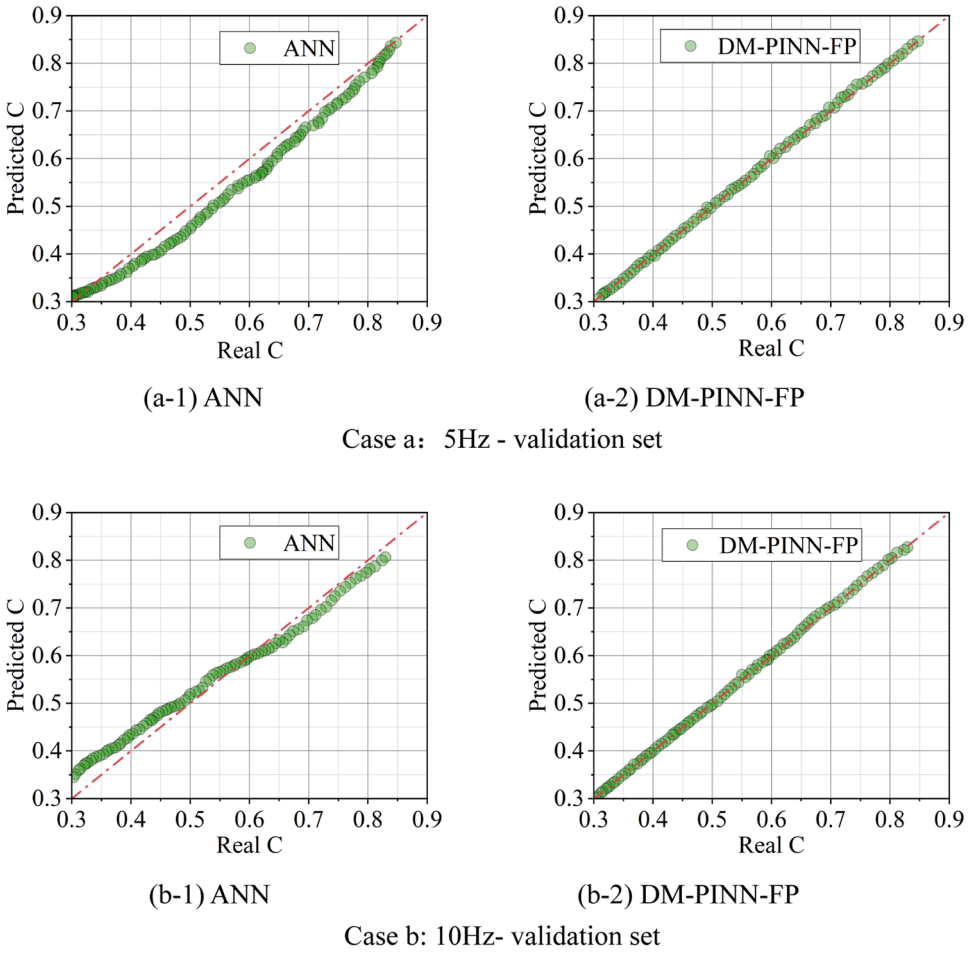

Fig. 6. Prediction accuracy of DM-PINN-FP and ANN.

values, while the vertical axis represents the predicted *C*values. Consequently, the closer the green points are to the $y = x$ line (red dashed line), the higher the prediction accuracy. Combining the distribution characteristics shown in Fig. 6, it can be concluded that the DM-PINN-FP outperforms the ANN. Its validation data points (green dots) are highly and densely clustered along the red dashed line, while the ANN exhibits varying degrees of prediction bias.

The performance of a network on a validation set with the same distribution as the training set cannot serve as definitive proof of its robustness. Furthermore, in practical engineering applications, it is often necessary to predict the full lifecycle of a material based on limited initial states. Therefore, the trained DM-PINN-FP and ANN models were employed to forecast the test C-S curves (25°C-400$\mu\varepsilon$-5Hz/10Hz). Using the first 15 points of the test curves as known data, the complete C-S curves were reconstructed through an iterative prediction process, where each predicted result was appended to the known sequence as input for the subsequent step.

Table 9
Performance metrics of DM-PINN-FP and ANN.

	DM-PINN-FP	ANN
25°C-400με-5Hz		
RMSE	0.0058	0.0569
MAE	0.0049	0.0439
R-square	0.9985	0.9211
25°C-400με-10Hz		
RMSE	0.0057	0.0396
MAE	0.0043	0.0374
R-square	0.9986	0.9430

Table 9 summarizes the evaluation metrics of both models on the two test curves. In Fig. 7, the green curves represent the experimental test data, while the red and blue curves denote the predictions from DM-PINN-FP and ANN, respectively. As evident from Table 9 and Fig. 7, the purely data-driven ANN model exhibits small errors in early-stage predictions but is highly susceptible to significant deviations in long-term forecasting due to error accumulation. Conversely, the proposed DM-PINN-FP model, by embedding mechanical constraints from VECD theory into the loss function, generates predictions that not only align closely with the experimental trajectories but also maintain exceptional reliability even toward the end of the curves. Moreover, because DM-PINN-FP and ANN were trained and tested using identical datasets, their comparison provides a controlled assessment of the contribution of the embedded physical constraints. The results demonstrate that the proposed framework effectively suppresses recursive prediction errors and preserves physically consistent stiffness degradation. This improvement arises from the combined effects of the dual-mode architecture, the monotonicity and cracking mode-consistency constraints, and the recurrent physical-boundary pathway.

4.3. Application of DM-PINN-FP

To further investigate how mesoscopic cracking modes influence the macroscopic fatigue response of asphalt mixtures, scenario analyses were performed using the trained DM-PINN-FP model. Aggregate type, temperature, and the corresponding β values were varied as model inputs to examine the response patterns learned by the model. It should be noted that the results presented in this section are model-based scenario

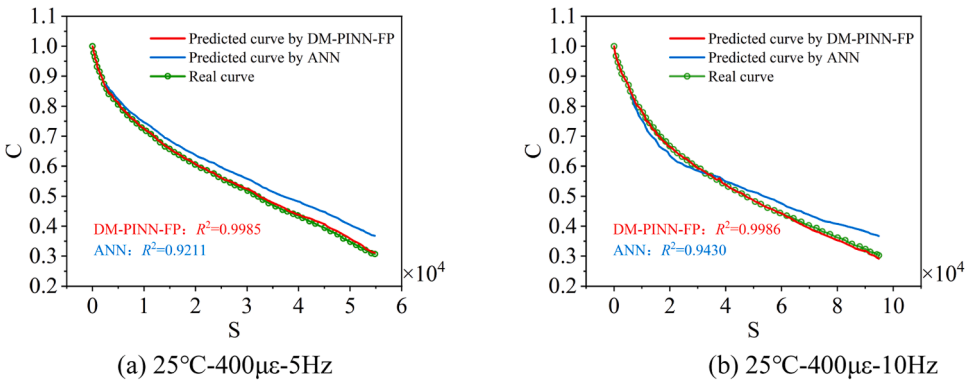

Fig. 7. Comparison between the predicted and the experimental C-S curves.

predictions intended to illustrate sensitivity trends, rather than independent experimental validation. For each test case, the first 15 points of a single C-S curve were used as initial known data. The differences in aggregate types and temperatures were reflected by varying the input values of β and temperature, thereby obtaining different evolution trends in the model-predicted curves. Since aggregate surface roughness is generally not considered in standard asphalt mixture design, the roughness was uniformly set to a constant value of $R = 0.0194$ mm in this section. The specific combinations of different conditions are summarized in Table 10.

As indicated in Table 10, under identical temperature and film thickness conditions, different aggregate types exhibit significant variations in their adhesion failure proportions β due to distinct surface physicochemical properties and interfacial bonding strengths. Specifically, the granite system shows a lower β, suggesting a greater tendency toward cohesive failure. In contrast, the β values for basalt and limestone systems are relatively close, indicating limited differences in their propensity for interfacial adhesive failure. The model-predicted C-S curves in Fig. 8 (a) demonstrate subtle distinctions in the stiffness degradation processes across different aggregate types. This illustrates that the DM-PINN-FP model can effectively identify variations in microscopic cracking mechanisms among different mineral systems and map them to macroscopic damage evolution behaviours. This result also validates the rationality of embedding the cracking sensitivity index into the dual-branch network architecture. To more intuitively reflect the influence of aggregate type on fatigue damage evolution, the predicted C-S curve for the limestone case (5°C, β= 0.48) was selected as the baseline to construct the pseudo-stiffness offset, ΔC, for other conditions, as shown in Fig. 8 (b). It can be observed from Fig. 8 (b) that the ΔC values induced by different aggregate types are generally small. This suggests that while mineral properties influence interfacial damage evolution via changes in the β value under consistent temperature and film thickness, their impact on the overall macroscopic C-S curve morphology is relatively limited, manifesting primarily as minor discrepancies during local degradation stages.

As the temperature rises from 5°C to 20°C, the β value increases significantly from 0.48 to 0.85. This trend indicates that elevated temperatures lead to the softening of the asphalt mastic and the weakening of interfacial bonding strength, making the material more susceptible to adhesion-dominated failure. When the temperature reaches 25°C, a fundamental shift in the dominant failure mode occurs. The C-S curves in Fig. 9 (a) reveal that at low-to-intermediate temperatures, the two cracking modes exhibit intense competition, resulting in a relatively gradual stiffness degradation. In contrast, at high temperatures, the accelerated attenuation of mastic strength leads to a marked reduction in the fatigue resistance of the asphalt mixture. As shown in Fig. 9 (b), the ΔC values induced by temperature variations increase significantly and exhibit an expanding trend as the damage variable S grows. This suggests that temperature not only modifies the cracking propensity index β but also substantially alters the global stiffness decay path by affecting the viscoelasticity of the asphalt mastic and the interfacial bonding state. Notably, at 25°C, the C-S curve shows the most pronounced offset, indicating that as the dominant failure mode gradually shifts toward cohesive failure, the material's fatigue resistance declines sharply. From the model prediction results, the influence of temperature on β and the fatigue evolution path is more direct and significant than other factors. Therefore, in practical engineering, priority should be given to the impact of service temperature on the fatigue performance of asphalt pavements.

Fig. 10 illustrates the evolution of fatigue life $\log(N_f)$ as a function of the Cracking Preference Index β under various operating conditions. the fatigue life is calculated based on VECD theory using the complete C-S curves predicted by the DM-PINN-FP model. In the calculation process, a 50% loss in pseudo-stiffness is defined as the fatigue failure threshold. Regarding the fundamental trend, all predicted curves exhibit a distinct single-peak characteristic regardless of changes in strain levels or loading frequencies; specifically, the fatigue life first increases and then decreases as β rises. At the critical point where β is approximately 0.48, the fatigue life reaches its peak across all conditions, suggesting that the synergistic evolution of cohesive and adhesive damage reaches a mechanical equilibrium, allowing the material to demonstrate optimal fatigue resistance. However, once β crosses this threshold and enters the Adhesion-dominated region, $\log(N_f)$ begins to decrease monotonically, which suggests that the intensification of interfacial adhesive failure directly undermines the macroscopic durability of the mixture.

Strain level exerts an extremely significant negative correlation on fatigue life. Observing the distribution of curves across different strain gradients in the figure, it is evident that as the strain level gradually increases from 5% to 20%, the $\log(N_f)$ curves undergo a drastic overall downward shift on the vertical axis, reflecting that high-strain loading significantly accelerates micro-crack propagation and damage accumulation. Notably, although changes in strain amplitude greatly compress the life span, they do not alter the fundamental morphology of the $\log(N_f)$ evolution or the position of the peak. This consistency indicates that the transition of mesoscopic damage modes characterized by the Cracking Preference Index β is highly robust, representing an

Table 10
Considered variables for the application of DM-PINN-FP.

Temperature/°C	Aggregate type	β/-
5	Limestone	0.48
	Granite	0.40
	Basalt	0.49
5	Limestone	0.48
10		0.58
15		0.70
20		0.85
25		0

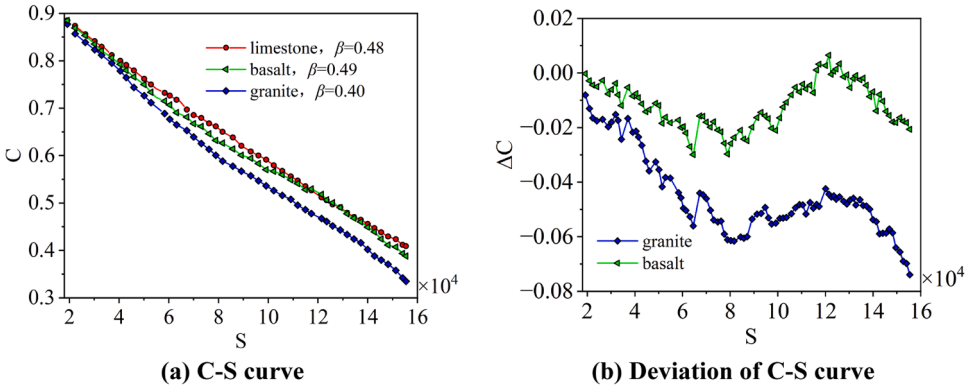

Fig. 8. Deviation caused by aggregate type based on DM-PINN-FP.

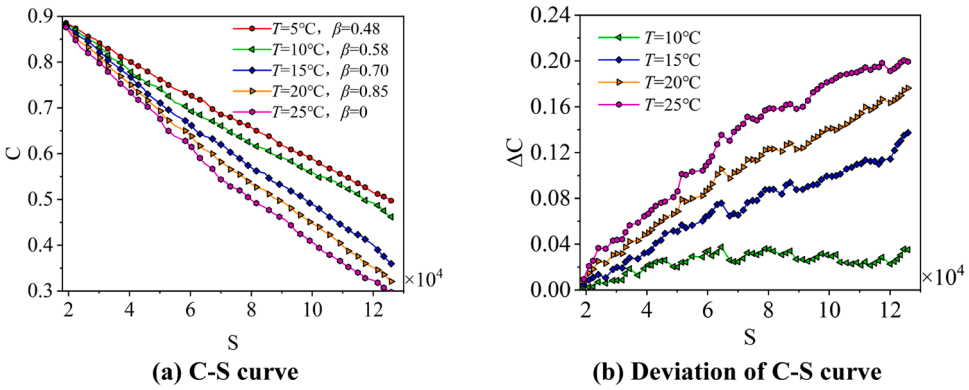

Fig. 9. Deviation caused by temperature based on DM-PINN-FP.

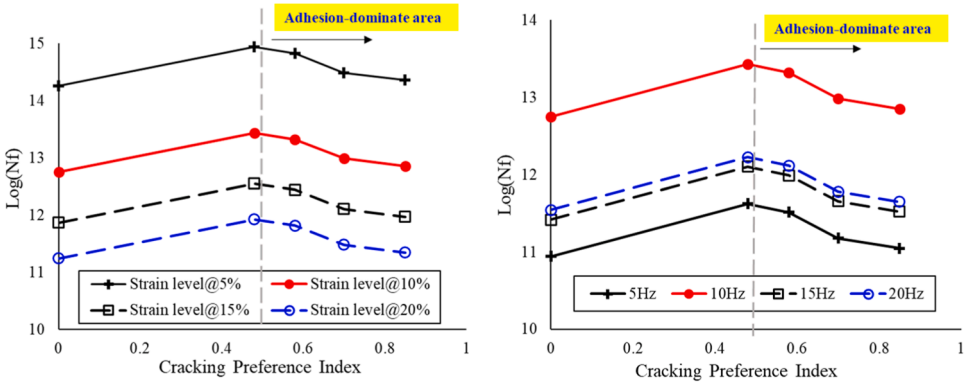

Fig. 10. Fatigue life calculated based on DM-PINN-FP.

intrinsic mechanical property of the material that remains unaffected by changes in external macroscopic load intensity.

The influence of loading frequency further reveals the viscoelastic characteristics of the asphalt mixture. Under the same β conditions, increasing the loading frequency (e.g., from 5Hz to 20Hz) generally causes the log(N_f) curves to lift, demonstrating the characteristic that higher frequencies lead to longer fatigue lives. This is because, under higher-frequency cyclic loading, the load duration on the material is shortened, and the asphalt mastic exhibits a higher dynamic modulus and stronger elastic recovery capability, thereby slowing down the rate of damage evolution. Like the impact of strain levels, fluctuations in loading frequency fail to shift the failure mode transition point at β =0.48. This further validates the accuracy of the DM-PINN-FP model in capturing microscopic cracking mechanisms and their macroscopic performance mapping under different dynamic loading conditions.

It should be emphasized that DM-PINN-FP is not inherently restricted to four-point bending fatigue tests. In principle, the framework can be extended to other fatigue test configurations, provided that a VECD-compatible C-S curve can be obtained and an initial degradation sequence is available as model input. Nevertheless, successful application to new material systems or environmental conditions requires recalibration of β to ensure that the relative contributions of adhesive and cohesive damage are appropriately represented.

5. Conclusions and recommendations

This study addresses the challenges of mesoscopic failure modes and macroscopic fatigue life prediction in asphalt mixtures by proposing a

mechanics-data dual-driven model, DM-PINN-FP, which incorporates a cracking propensity index. This framework achieves a unified representation from mesoscopic damage modes to macroscopic fatigue performance. The primary conclusions are as follows:

(1). Based on pull-off tests, an interfacial adhesion cracking propensity parameter and a fatigue cracking sensitivity index were developed. This approach enables the quantitative characterization of interfacial failure modes and demonstrates robust applicability across limestone, granite, and basalt systems.
(2). A dual-mode physical model describing the synergistic evolution of cohesive and adhesive damage was derived and embedded into a neural network architecture. The resulting DM-PINN-FP model balances physical interpretability with data-fitting capabilities, achieving high-precision predictions of C-S curves using only initial fatigue test data. It is expected to reduce the number of full-duration fatigue tests required for preliminary mixture screening and comparative parametric studies.
(3). The analysis demonstrates that aggregate type, temperature, and asphalt film thickness significantly affect β and, consequently, the relative dominance of adhesive and cohesive cracking. By incorporating β into the dual-mode framework, the model captures the transition between the two cracking mechanisms under different conditions and establishes a clear relationship between cracking preference and fatigue life. The explicit separation of adhesive and cohesive damage further provides mechanism-based guidance for targeted mixture design and performance optimization.

Despite the promising predictive performance of the proposed model, there remains room for further expansion. Future research could incorporate modified asphalt, recycled mixtures, and various gradations to verify the model's generalization capability in complex systems. Furthermore, integrating advanced mesoscopic characterization techniques, such as CT scanning and Digital Image Correlation (DIC), could further refine the physical definition of β and the underlying damage mechanisms.

CRediT authorship contribution statement

Quan Liu: Writing – review & editing, Supervision, Methodology, Funding acquisition, Conceptualization. **Huimin Li:** Writing – original draft, Visualization, Software, Investigation, Formal analysis, Data curation. **Yangming Gao:** Writing – review & editing, Supervision, Conceptualization. **Hanyu Zhang:** Methodology, Conceptualization. **Yuanyuan Li:** Methodology, Conceptualization. **Denise Lee:** Project administration, Conceptualization. **Jiantao Wu:** Supervision.

Declaration of competing interest

The authors declare that they have no known competing financial interests or personal relationships that could have appeared to influence the work reported in this paper.

Acknowledgment

The authors gratefully acknowledge the financial support from the National Natural Science Foundation of China (Grant No. 52408477) and the Marie Skłodowska-Curie Actions (MSCA) program with grant agreement (No. 101210582).

Data availability

Data will be made available on request.

References

Alnaqbi, A. J., Zeiada, W., Al-Khateeb, G., Abttan, A., & Abuzwidah, M. (2024). Predictive models for flexible pavement fatigue cracking based on machine learning. *Transportation Engineering, 16*. https://doi.org/10.1016/j.treng.2024.100243

Azarhoosh, A., Moghadas Nejad, F., & Khodaii, A. (2017). The influence of cohesion and adhesion parameters on the fatigue life of hot mix asphalt. *The Journal of Adhesion, 93*(13), 1048–1067.

Błażejowski, K., Wójcik-Wiśniewska, M., Baranowska, W., Ostrowski, P., Černý, R., & Jisa, P. (2020). Fatigue performance of bituminous binders tested by linear amplitude sweep test. In *Proceedings of the 5th International Symposium on Asphalt Pavements & Environment (Ape)* (pp. 385–394).

Cao, W., & Wang, C. (2019). Fatigue performance characterization and prediction of asphalt binders using the linear amplitude sweep based viscoelastic continuum damage approach. *International Journal of Fatigue, 119*, 112–125. https://doi.org/10.1016/j.ijfatigue.2018.09.028

Chen, J., & Liu, Y. (2022). Fatigue modeling using neural networks: A comprehensive review. *Fatigue & Fracture of Engineering Materials & Structures, 45*(4), 945–979. https://doi.org/10.1111/ffe.13640

Chen, P., Luo, X., Gao, Y., & Zhang, Y. (2022). Modeling percentages of cohesive and adhesive debonding in bitumen-aggregate interfaces using molecular dynamics approaches. *Applied Surface Science, 571*. https://doi.org/10.1016/j.apsusc.2021.151318

Cheng, H., Sun, L., Wang, Y., Liu, L., & Chen, X. (2022). Fatigue test setups and analysis methods for asphalt mixture: A state-of-the-art review. *Journal of Road Engineering, 2*(4), 279–308. https://doi.org/10.1016/j.jreng.2022.11.002

Cong, L., Peng, J., Guo, Z., & Wang, Q. (2017). Evaluation of fatigue cracking in asphalt mixtures based on surface energy. *Journal of Materials in Civil Engineering, 29*(3), Article D4015003.

Deng, Y., Wang, H., & Shi, X. (2024). Physics-guided neural network for predicting asphalt mixture rutting with balanced accuracy, stability and rationality. *Neural Networks, 172*, Article 106085. https://doi.org/10.1016/j.neunet.2023.12.039

Dong, Y., Yang, X., Chang, D., & Li, Q. (2025). Predicting fatigue life of multi-defect materials using the fracture mechanics-based physics-informed neural network framework. *International Journal of Fatigue, 190*. https://doi.org/10.1016/j.ijfatigue.2024.108626

Du, C., Sun, Y., Chen, J., Gong, H., Wei, X., & Zhang, Z. (2020). Analysis of cohesive and adhesive damage initiations of asphalt pavement using a microstructure-based finite element model. *Construction and Building Materials, 261*. https://doi.org/10.1016/j.conbuildmat.2020.119973

Fahad, M., & Bektas, N. (2025). Data-driven pavement performance: Machine learning-based predictive models. *Applied Sciences, 15*(7). https://doi.org/10.3390/app15073889

Fan, X., Lv, S., Xia, C., Ge, D., Liu, C., & Lu, W. (2024). Strength prediction of asphalt mixture under interactive conditions based on bpnn and svm. *Case Studies in Construction Materials, 21*. https://doi.org/10.1016/j.cscm.2024.e03489

Feng, L., Li, Z., Huang, W., Guo, W., Liu, H., & Han, S. (2026). A dual-pathway physics-informed neural network approach for fatigue crack growth prediction under temperature-dependent r-effect. *International Journal of Fatigue, 208*. https://doi.org/10.1016/j.ijfatigue.2026.109573

Fuhg, J. N., Hamel, C. M., Johnson, K., Jones, R., & Bouklas, N. (2023). Modular machine learning-based elastoplasticity: Generalization in the context of limited data. *Computer Methods in Applied Mechanics and Engineering, 407*. https://doi.org/10.1016/j.cma.2023.115930

Gong, X., Gu, H., Yan, H., Huang, X., Zhou, H., & Ma, J. (2025). Effect of aggregate roughness and film thickness on interfacial interaction of aggregate-asphalt-aggregate films. *Construction and Building Materials, 486*. https://doi.org/10.1016/j.conbuildmat.2025.141984

Han, C., Zhang, J., Tu, Z., & Ma, T. (2024). Pinn-Afp: A novel c-s curve estimation method for asphalt mixtures fatigue prediction based on physics-informed neural network. *Construction and Building Materials, 415*. https://doi.org/10.1016/j.conbuildmat.2024.135070

Hosseini, S. A., & Smadi, O. (2021). How prediction accuracy can affect the decision-making process in pavement management system. *Infrastructures, 6*(2). https://doi.org/10.3390/infrastructures6020028

Houlík, J., Valentin, J., & Nežerka, V. (2026). Predicting the fatigue life of asphalt concrete using neural networks. *Journal of Materials in Civil Engineering, 38*(4). https://doi.org/10.1061/jmcee7.Mteng-20929

Isied, M. M., & Souliman, M. I. (2019). Integrated predictive artificial neural network fatigue endurance limit model for asphalt concrete pavements. *Canadian Journal of Civil Engineering, 46*(2), 114–123. https://doi.org/10.1139/cjce-2018-0051

Karniadakis, G. E., Kevrekidis, I. G., Lu, L., Perdikaris, P., Wang, S., & Yang, L. (2021). Physics-informed machine learning. *Nature Reviews Physics, 3*(6), 422–440. https://doi.org/10.1038/s42254-021-00314-5

Kim, Y.-R., Little, D. N., & Lytton, R. L. (2004). Effect of moisture damage on material properties and fatigue resistance of asphalt mixtures. *Transportation Research Record, 1891*(1), 48–54.

Li, J., Zhang, S., & Wang, X. (2025). Physics-informed neural network with fuzzy partial differential equation for pavement performance prediction. *Automation in Construction, 171*. https://doi.org/10.1016/j.autcon.2025.105983

Li, Y., Li, Q., Zhou, S., Wang, C., Zhang, D., Liu, Q., Jiang, G., Zhu, H., & Zhou, X. (2026). Manufacturing process optimization and multi-mechanism stability regulation of high-performance emulsified asphalt. *Construction and Building Materials, 535*. https://doi.org/10.1016/j.conbuildmat.2026.146936

Liao, W., Long, X., & Jiang, C. (2025). A physics-informed neural network method for identifying parameters and predicting remaining life of fatigue crack growth.

International Journal of Fatigue, 191. https://doi.org/10.1016/j.ijfatigue.2024.108678

Lucas Júnior, J. L. O., Babadopulos, L. F. D. A. L., & Soares, J. B. (2020). Influence of aggregate–binder adhesion on fatigue life of asphalt mixtures. *Journal of Testing and Evaluation, 48*(1), 150–160.

Luo, X., Huang, J., Shen, L., Wang, H., & Shi, Z. (2026). Physics-informed neural networks for constitutive modeling and multiphysics coupling in viscoelastic materials: Applications to asphalt pavement mechanics. *Neural Networks, 200*, Article 108803. https://doi.org/10.1016/j.neunet.2026.108803

Luo, X., Luo, R., & Lytton, R. L. (2015). Energy-based crack initiation criterion for viscoelastoplastic materials with distributed cracks. *Journal of Engineering Mechanics, 141*(2). https://doi.org/10.1061/(asce)em.1943-7889.0000830

Luo, X., Zhang, Y., & Lytton, R. L. (2015). Implementation of pseudo j-integral based Paris' law for fatigue cracking in asphalt mixtures and pavements. *Materials and Structures, 49*(9), 3713–3732. https://doi.org/10.1617/s11527-015-0750-z

Luo, Y., Wu, H., Song, W., Yin, J., Zhan, Y., Yu, J., & Abubakar Wada, S. (2023). Thermal fatigue and cracking behaviors of asphalt mixtures under different temperature variations. *Construction and Building Materials, 369*. https://doi.org/10.1016/j.conbuildmat.2023.130623

Lytton, R.L., Masad, E.A., Zollinger, C., Bulut, R. & Little, D.N. (2005), Measurements of surface energy and its relationship to moisture damage.

Mazeika, M., Phan, L., Yin, X., Zou, A., Wang, Z., Mu, N., Sakhaee, E., Li, N., Basart, S., Li, B., Forsyth, D., & Hendrycks, D. (2024). Harmbench: A standardized evaluation framework for automated red teaming and robust refusal. In *Proceedings of the 41st International Conference on Machine Learning* (p. 1431). Vienna, Austria: JMLR. Article.

Park, S. W., Kim, Y. R., & Schapery, R. A. (1996). A viscoelastic continuum damage model and its application to uniaxial behavior of asphalt concrete. *Mechanics of Materials*.

Raissi, M., Perdikaris, P., & Karniadakis, G. E. (2019). Physics-informed neural networks: A deep learning framework for solving forward and inverse problems involving nonlinear partial differential equations. *Journal of Computational Physics, 378*, 686–707. https://doi.org/10.1016/j.jcp.2018.10.045

Shen, S., Airey, G. D., Carpenter, S. H., & Huang, H. (2011). A dissipated energy approach to fatigue evaluation. *Road Materials and Pavement Design, 7*(1), 47–69. https://doi.org/10.1080/14680629.2006.9690026

Shi, B., Liu, Q., Gao, Y., Wu, J., & Chen, J. (2023). Analysis of the cohesion/adhesion proportion around bitumen-mineral failure interface under tensile loading. *Construction and Building Materials, 399*. https://doi.org/10.1016/j.conbuildmat.2023.132555

Shin, H., Yoon, T., & Yoon, S. (2025). Fatigue life predictor: Predicting fatigue life of metallic material using lstm with a contextual attention model. *RSC Adv, 15*(20), 15781–15795. https://doi.org/10.1039/d5ra01578b

Siegel, J. W. (2025). Advancing physical understanding with interpretable machine learning. *Physics, 18*. https://doi.org/10.1103/Physics.18.199

Sun, Y., He, D., & Li, J. (2021). Research on the fatigue life prediction for a new modified asphalt mixture of a support vector machine based on particle swarm optimization. *Applied Sciences, 11*(24). https://doi.org/10.3390/app112411867

Sun, Z., Li, S., Zhang, J., & Zeng, Y. (2020). Adhesion property of bituminous crack sealants to different asphalt mixtures based on surface energy theory. *Construction and Building Materials, 261*. https://doi.org/10.1016/j.conbuildmat.2020.120006

Ulloa, N., José Allauca, P., Pozo, E., Ramesh, G., Rajesh, S., & Mayakannan, S. (2023). Ann based fatigue life assessment of Fsw on Aa2219-T351 and optimization of welding parameter. *Materials Today: Proceedings*. https://doi.org/10.1016/j.matpr.2023.05.480

Underwood, B. S., Kim, Y. R., & Guddati, M. N. (2010). Improved calculation method of damage parameter in viscoelastic continuum damage model. *International Journal of Pavement Engineering, 11*(6), 459–476. https://doi.org/10.1080/10298430903398088

Wang, J., Cao, S., Luo, X., & Zhang, Y. (2024). Characterizing bitumen-aggregate interfacial failures under coupled size effects of bitumen film thickness and aggregate surface roughness. *Construction and Building Materials, 416*. https://doi.org/10.1016/j.conbuildmat.2024.135238

Zeiada, W., Obaid, L., El-Badawy, S., Abd El-Hakim, R., & Awed, A. (2025). Benchmarking classical and deep machine learning models for predicting hot mix asphalt dynamic modulus. *Civil Engineering Journal, 11*(1), 76–106. https://doi.org/10.28991/cej-2025-011-01-06

Zhang, J., Airey, G. D., & Grenfell, J. R. A. (2015). Experimental evaluation of cohesive and adhesive bond strength and fracture energy of bitumen-aggregate systems. *Materials and Structures, 49*(7), 2653–2667. https://doi.org/10.1617/s11527-015-0674-7

Zhang, J., Wang, Y. D., & Su, Y. (2019). Fatigue damage evolution model of asphalt mixture considering influence of loading frequency. *Construction and Building Materials, 218*, 712–720. https://doi.org/10.1016/j.conbuildmat.2019.05.029

Zhang, Y., Luo, X., Luo, R., & Lytton, R. L. (2014). Crack initiation in asphalt mixtures under external compressive loads. *Construction and Building Materials, 72*, 94–103. https://doi.org/10.1016/j.conbuildmat.2014.09.009

Zhu, M., Zhang, H., Jiao, A., Karniadakis, G. E., & Lu, L. (2023). Reliable extrapolation of deep neural operators informed by physics or sparse observations. *Computer Methods in Applied Mechanics and Engineering, 412*. https://doi.org/10.1016/j.cma.2023.116064

Zhu, Y., Hu, Z., Luo, J., & Song, P. (2024). Probabilistic fatigue life prediction using multi-layer perceptron with maximum entropy algorithm. *International Journal of Fatigue, 187*, Article 108445.